

---

# SAM-REF: RETHINKING IMAGE-PROMPT SYNERGY FOR REFINEMENT IN SEGMENT ANYTHING

---

A PREPRINT

**Chongkai Yu**  
MT Lab, Meitu Inc

**Anqi Li**  
Beijing Institute of Technology

**Xiaochao Qu**  
MT Lab, Meitu Inc

**Luoqi Liu**  
MT Lab, Meitu Inc

**Ting Liu\***  
MT Lab, Meitu Inc

August 23, 2024

## ABSTRACT

The advent of the Segment Anything Model (SAM) marks a significant milestone for interactive segmentation using generalist models. As a *late fusion* model, SAM extracts image embeddings once and merges them with prompts in later interactions. This strategy limits the models' ability to extract detailed information from the prompted target zone. Current specialist models utilize the *early fusion* strategy that encodes the combination of images and prompts to target the prompted objects, yet repetitive complex computations on the images result in high latency. The key to these issues is efficiently synergizing the images and prompts. We propose SAM-REF, a two-stage refinement framework that fully integrates images and prompts globally and locally while maintaining the accuracy of early fusion and the efficiency of late fusion. The first-stage GlobalDiff Refiner is a lightweight early fusion network that combines the whole image and prompts, focusing on capturing detailed information for the entire object. The second-stage PatchDiff Refiner locates the object's detail window according to the mask and prompts, then refines the local details of the object. Experimentally, we demonstrated the high effectiveness and efficiency of our method in tackling complex cases with multiple interactions. Our SAM-REF model outperforms the current state-of-the-art method in most metrics on segmentation quality without compromising efficiency.

**Keywords** Interactive Segmentation · SAM

## 1 Introduction

Interactive segmentation Liu et al. [2024], Huang et al. [2024a], Kirillov et al. [2023], Chen et al. [2022], Huang et al. [2023] is a crucial task in computer vision that has garnered significant attention from both academia and industry. It leverages user input through simple interactions, such as scribbles, boxes, and clicks, to conveniently obtain accurate masks. Recently, the Segment Anything Model (SAM) Kirillov et al. [2023] has been introduced as a foundational vision model for general image segmentation. Trained with billion-scale mask labels, it demonstrates impressive generalization and efficiency when processing various types of prompts.

SAM alongside the concurrent InterFormerHuang et al. [2023] has pioneered a late fusion pipeline for interactive segmentation. As shown in Fig 1, the pipeline utilizes a powerful image encoders, Vision Transformers (ViTs) Li et al. [2022], to generates image embeddings for all objects within the same image. Prompts(e.g. clicks) are combined with image embeddings only during interaction and fed into a lightweight decoder to generate segmentation masks.

---

\*Use footnote for providing further information about author (webpage, alternative address)—*not* for acknowledging funding agencies.

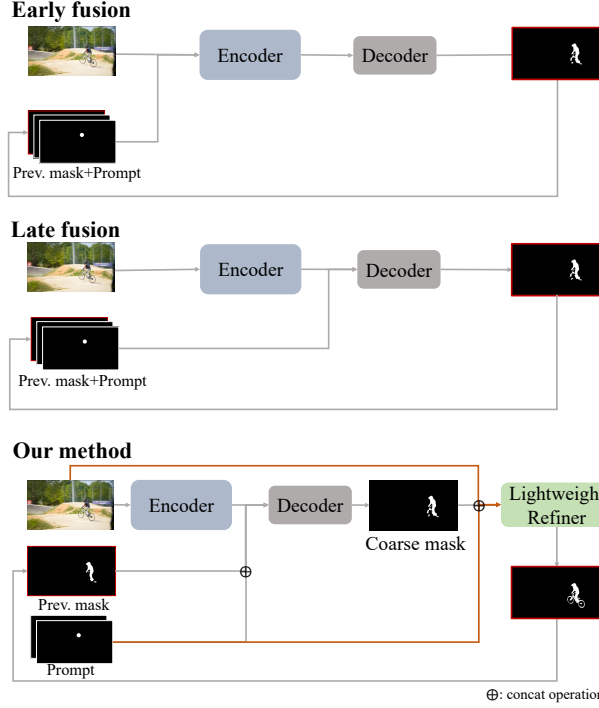


Figure 1: **Comparison of the pipeline between our method and two other methods.** Our method strikes a balance between the detail enhancement achieved through early fusion of images and prompt collaboration, and the efficiency of avoiding redundant feature extraction in late fusion.

This pipeline avoids redundant image feature extraction, significantly improving both training and inference efficiency. However, this approach is often unsatisfactory in many complex scenarios.

In contrast, specialist models such as FocalClickChen et al. [2022], SimpleClickLiu et al. [2023], and CFRSun et al. [2024] jointly encode the image and prompts to generate features specifically for the objects during interaction. For complex and challenging cases, these traditional early-fusion pipelines often achieve better results in capturing thin object structures and fine details than late fusion pipeline.

**How to balance and address the limitations between the two pipelines?** The key issue for interactive segmentation is the efficient synergy between the image and prompts. Although early fusion pipeline emphasizes the synergy between the image and the prompt, it fails to address issues of latency and generalization. In comparison to SAM, single point and random points perform worseKirillov et al. [2023]. On the other hand, late fusion pipeline entirely discards the interaction between the original image and the prompt. Despite the ability of a powerful image encoder to focus on all objects, it struggles to capture their fine details. Subsequent finetune approachesKe et al. [2024], Huang et al. [2024a], Xie et al. [2024] based on SAM are also limited by the image embeddings, ignoring the crucial synergy between the image and the prompt. Additionally, the sparse representation of visual prompts in SAM also limits high-quality segmentation resultsLiu et al. [2024].

Therefore, we propose a lightweight refinement approach called SAM-REF that reintegrates the prompt and the image while maintaining the efficiency of late fusion pipeline. Our approach introduces two key modules to progressively refine SAM’s mask without altering the original SAM structure. First, SAM outputs a coarse mask, which is then combined with the prompt and image into a dense map. This dense map matches the spatial dimensions of the image, better preserving the detailed spatial attributes of the visual prompts(e.g. clicks)Liu et al. [2024]. In fact, this map can also support other prompts such as scribbles and boxes, but these are beyond the scope of this paper and thus are not discussed in detail. Next, GlobalDiff Refiner utilizes a lightweight network to capture detailed information of the entire object while incorporating SAM embeddings to leverage its strong semantic capabilities. Finally, we refine the global mask by predicting the error map and the detail map. Additionally, we introduce PatchDiff Refiner to further enhance the capability of local detail refinement. It is able to update local details based on changes in the GlobalDiff’s error map.

Experimentally, SAM-REF fully exploits the potential of SAM for interactive segmentation. On benchmark datasets, our method achieves state-of-the-art performance in NoC90 and matches the top-performing method (SimpleClickLiu

et al. [2023]) in NoC95 with higher efficiency. On high-quality segmentation datasets, our method outperforms previous methods in both quantitative and qualitative analyses while maintaining SAM’s low latency advantage in the Segment Anything Task (SAT).

We summarize our contributions as follows:

- We introduce SAM-REF, a new pipeline that reintegrates the prompt and the image to capture object details while maintaining efficiency.
- SAM-REF is composed of GlobalDiff Refiner for global detail adjustment and PatchDiff Refiner for dynamic window refinement.
- SAM-REF achieves state-of-the-art performance on various datasets while maintaining SAM’s low latency advantage.

## 2 Related Work

### 2.1 Early Fusion Interactive Segmentation

In deep learning LeCun et al. [2015], early fusion strategy Barnum et al. [2020] means combining different information in the early stages of networks. In segmentation tasks, early fusion interactive segmentation combines the image with interactive information before processing them through deeper network layers, *e.g.* ViTDosovitskiy et al. [2020], allowing for more refined and contextually aware segmentation results. The first deep-learning-based interactive segmentation model, DIOS Xu et al. [2016], takes the early fusion strategy by embedding positive and negative clicks into distance maps and concatenating them with the original image as input. RITM Sofiuk et al. [2022] introduces concatenating the previous mask with point maps, and later works mostly follow this approach. Many methods have been used to improve accuracy. FocalClick Chen et al. [2022] and FocusCut Lin et al. [2022] use local refinement, and CFR Sun et al. [2024] uses cascade refinement. SimpleClick Liu et al. [2023] up-sample the image feature, and PseudoClick Liu et al. [2022] simulates an additional prompt. Though high precision, the high latency of early fusion has always been a problem. FocalClick Chen et al. [2022] compresses the size of the feature to speed up while losing some accuracy.

### 2.2 Late Fusion Interactive Segmentation

Late fusion interactive segmentation extracts image embeddings once and combines them with interactive prompts in later interactions. Interformer Huang et al. [2023] and SAM Kirillov et al. [2023] decouple the light prompt encoder and the decoder from the heavy encoder, accelerating the speed. However, late fusion cannot catch details according to the focusless embeddings, leading to a lack of precision. To promote accuracy, SegNext Liu et al. [2024] adds dense representation and fusion of visual prompts to extract more visual information, FocSAM Huang et al. [2024a] introduces window-based attention to focus on the target zone of embeddings, while HQ-SAM Ke et al. [2024] uses global-local fusion and proposed HQ-SAM dataset with high quality. These methods aim to explore more information from the embeddings. However, the embeddings may not have enough detailed information about the target zone, so these methods cannot achieve significant improvements in accuracy. In contrast, our method combines early fusion and late fusion, extracting detailed information from the image directly.

## 3 Method

We propose SAM-REF to further exploit the potential of SAM. We first briefly review the architecture of SAM and introduce the overview of SAM-REF pipeline. Then we provide a detailed explanation of GlobalDiff Refiner and PatchDiff Refiner. Finally, we discuss the training loss.

### 3.1 Preliminaries: SAM

SAM consists of three modules: an image encode, a prompt encode, and a mask decode. **Image encoder:** a heavy ViT-based backbone is structured into four stages, each of equal depth, and employs window-based attention in each stage to enhance computational efficiency Li et al. [2022]. **Prompt encoder:** in the interaction phase, it transforms the positional information of the input boxes, clicks, and masks into embeddings. However, the sparse representations of visual prompts, similar to those used in linguistic prompts, may inhibit the ability to capture images details Liu et al. [2024]. **Mask decoder:** It combines image embeddings and prompt embeddings through a two-layer transformer-based decoder to predict the final masks.

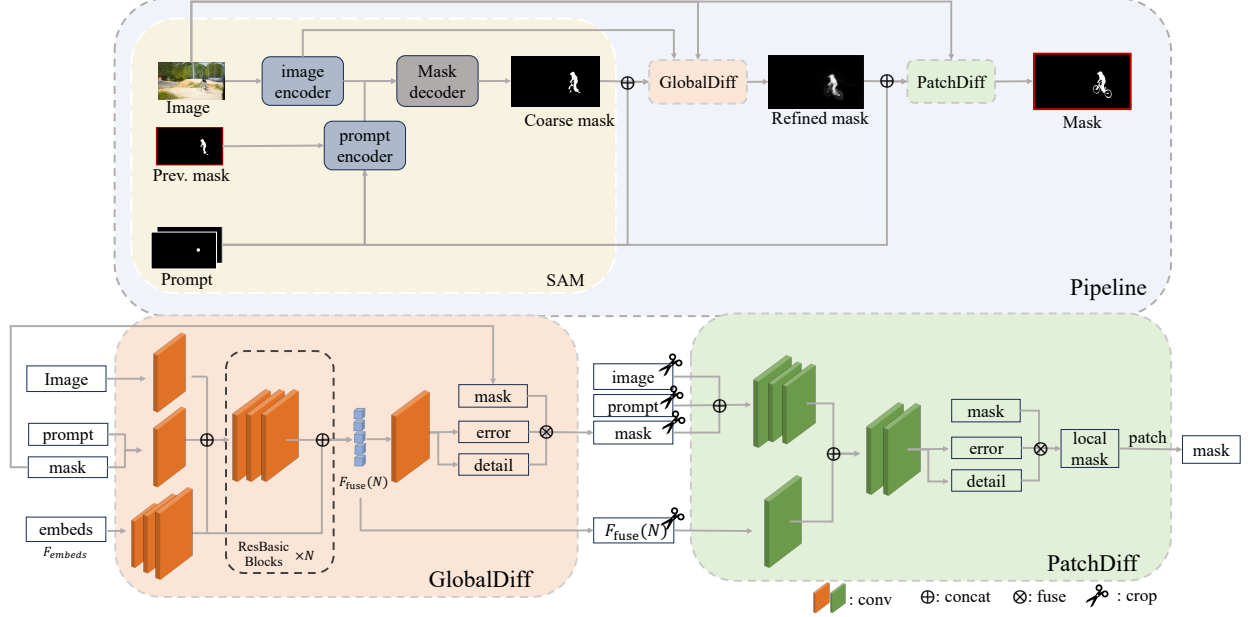


Figure 2: **The framework of the proposed SAM-REF.** SAM initially uses a late fusion approach to combine the encoded image with the prompt, producing a coarse mask. We first use SAM to extract image embeddings and generate a coarse mask. With the image embeddings, the coarse mask, and the prompt, GlobalDiff Refiner incorporates the image to extract detailed original information by a lightweight network, refining the coarse mask. The PatchDiff Refiner crops a local region according to the prompt and the masks, refines the local region, and patches it back without changing the details in other areas. The detailed framework and method will be discussed in Method.

During the interaction process, the prompt encoder and mask decoder are lightweight, and the heavy image encoder only needs to be performed once before the interaction. Therefore, the entire inference pipeline is very efficient.

### 3.2 Ours: SAM-REF

To preserve the inherent structure of SAM while fully exploiting its potential, we adopt a decoupled design approach wherever possible. To this end, SAM-REF introduces two new key components to refine the mask progressively.

The overall architecture of SAM-REF is shown in Fig 2. Initially, SAM uses a late fusion approach to combine the encoded image with the prompt, producing a coarse mask. Afterwards, GlobalDiff Refine directly combines the prompt with the image and extracts detailed information about the prompted target through a lightweight convolutional network. Meanwhile, it progressively incorporates SAM’s image embeddings at each stage to preserve SAM’s robust deep semantic capabilities, thus refining the overall objects.

For the local region around the prompt, PatchDiff Refiner combines the prompt with the cropped image of that region for localized refinement. It adaptively updates and modifies regions based on changes in the error map from the previous module, while preserving details in other areas.

### 3.3 GlobalDiff Refiner

#### 3.3.1 Image-Prompt Fusion

First, we need to efficiently fuse the prompt and the image. Follow Liu et al. [2024], Sofiuk et al. [2022], Benenson et al. [2019], We adopt the method of encoding click prompts as disks with a small radius to obtain the dense map of the visual prompts. Unlike before, this map now has three channels: besides the positive prompt map and the negative prompt map, the mask map from the previous prediction is replaced by the coarse logits output by SAM in the current interaction. We adopt the method from RITMSofiuk et al. [2022], utilizing two convolutions to align the scale and channels of the image  $I_{ori} \in \mathbb{R}^{3 \times 1024 \times 1024}$  and dense map  $P_{ori} \in \mathbb{R}^{3 \times 256 \times 256}$ , then summing them to obtain an initial fused feature  $F_{fuse}(0) \in \mathbb{R}^{64 \times 256 \times 256}$ .

Table 1: **Comparison of SPC, NoC90 and NoC95 with previous methods.** We report the results on the mainstream datasets. The superscript \* on the datasets indicates the model is fine-tuned on that dataset. Our SAM-REF model achieves high performance with fast speed.

Method	Train data	Backbone	SPC↓	Grabcut		Berkeley		DAVIS		SBD	
				NoC90	NoC95	NoC90	NoC95	NoC90	NoC95	NoC90	NoC95
<i>Early Fusion</i>											
RITM	COCO+LVIS	HRNet18	-	1.54	2.22	2.26	6.46	5.74	12.45	6.05	12.47
RITM	COCO+LVIS	HRNet32	-	1.56	2.48	2.10	5.41	5.34	11.52	5.71	12.00
PseudoClick	COCO+LVIS	HRNet32	-	1.50	-	2.08	-	5.11	-	5.54	-
FocalClick	COCO+LVIS	SegF-B3-S2 <sub>384</sub>	0.232	1.68	1.92	1.71	4.21	4.90	10.40	5.59	11.91
SimpleClick	COCO+LVIS	ViT-H	8.24	1.50	<b>1.66</b>	1.75	4.34	4.78	<b>8.88</b>	4.70	10.76
<i>Late Fusion</i>											
InterFormer	COCO+LVIS	ViT-B	0.153	1.50	-	3.14	-	6.19	-	6.34	-
InterFormer	COCO+LVIS	ViT-L	0.271	1.36	-	2.53	-	5.21	-	5.51	-
SAM	SA-1B	ViT-H	0.413	1.88	2.18	2.09	5.14	5.19	10.00	7.62	15.03
SAM-HQ	HQ-Seg*	ViT-H	0.443	1.86	2.16	2.14	4.94	5.06	9.65	7.91	15.08
FocSAM	COCO+LVIS*	ViT-H	0.467	1.44	2.60	1.50	3.44	4.76	10.77	5.07	11.67
Ours	COCO+LVIS*	ViT-B	0.278	1.40	2.54	1.58	3.73	<b>4.75</b>	10.55	5.56	11.86
Ours	COCO+LVIS*	ViT-H	0.511	<b>1.36</b>	2.36	<b>1.43</b>	<b>3.18</b>	<b>4.56</b>	9.28	<b>4.44</b>	<b>10.61</b>

### 3.3.2 Global Detail Extractor

We hypothesize that SAM, relying on the powerful ViT architecture, has already learned deep semantic information [Huang et al. (2024b)]. The primary deficiency lies in its understanding of low-level details. To maintain SAM’s semantic understanding and design an efficient detail extraction module, we employ a scale-invariant convolutional structure and integrate it with SAM image embeddings  $\mathbf{F}_{embeds} \in \mathbb{R}^{256 \times 64 \times 64}$ .

Specifically, as illustrated in Fig 2, we progressively upscale the SAM image embeddings  $\hat{\mathbf{F}}_{embeds} \in \mathbb{R}^{64 \times 256 \times 256}$  and add them to the feature map  $\mathbf{F}_{fuse}(0) \in \mathbb{R}^{64 \times 256 \times 256}$ . Subsequently, we utilize a scale-invariant ResBasicBlock [He et al. (2016)] to capture fine details. This process is repeated multiple times  $N$ , with each iteration merging with the SAM image embeddings to prevent the loss of deep semantic information from SAM.

### 3.3.3 Error-Detail Refinement

Following the Global Detail Extractor, we reduce the number of channels in feature map  $\mathbf{F}_{fuse}(N) \in \mathbb{R}^{64 \times 256 \times 256}$  and apply a 1x1 convolution layer for decoding. To maintain the integrity of SAM segmentation, we predict the error map  $\mathbf{M}_e^g$  and the detail map  $\mathbf{M}_d^g$  to modify error-prone regions. The final prediction map  $\mathbf{M}_r^g$  is obtained as shown in Equation 1.

$$\mathbf{M}_r^g = \text{Sigmoid}(\mathbf{M}_e^g) * \mathbf{M}_d^g + (1 - \text{Sigmoid}(\mathbf{M}_e^g)) * \mathbf{M}_c^s \quad (1)$$

Where  $\mathbf{M}_c^s$  is the prediction result of SAM, and  $\mathbf{M}_e^g$  is supervised by the error regions between the ground truth and the binary mask generated by thresholding  $\mathbf{M}_c^s$  at 0.5. After GlobalDiff Refiner, we obtained the global refinement of the objects.

## 3.4 PatchDiff Refiner

### 3.4.1 PatchDiff Refinement

In this module, we perform prompt and image fusion again for the user-interacted local regions to refine the local details of the objects. Inspired by FocalClick [Chen et al. (2022)], we calculate the max connected component of the difference between the GlobalDiff Refiner result and the previous mask. Subsequently, we generate the external box for the connected component that includes the last prompt and proportionally expand it. The specific design is illustrated in Fig 2.

In contrast to focalclick, we use RoiAlign [He et al. (2017)] to crop the logits and the fused feature  $\mathbf{F}_{fuse}(N)$  from GlobalDiff Refiner. Additionally, our two prediction heads generate the detail map and the error map based on the local SAM predictions, rather than the boundary map. The local refined Mask  $\mathbf{M}_r^l$  updating is performed as outlined in Eq 2.

$$\mathbf{M}_r^l = \text{Sigmoid}(\mathbf{M}_e^p) * \mathbf{M}_d^p + (1 - \text{Sigmoid}(\mathbf{M}_e^p)) * \mathbf{M}_c^p \quad (2)$$

where  $\mathbf{M}_c^p$  is the local prediction result of SAM,  $\mathbf{M}_e^p$ ,  $\mathbf{M}_d^p$  represent the predictions for local error and detail maps.

Table 2: **Results on high-quality data.** All of the models are evaluated on the HQ-Seg dataset. The superscript \* on the datasets indicates the model is fine-tuned on that dataset.

Method	Train data	Backbone	Latency(s)↓	5-mIoU↑	NoC90↓	NoC95↓	NoF95↓
FocalClick	COCO+LVIS	SegF-B3-S2 <sub>256</sub>	30.85	84.63	8.12	12.63	835
FocalClick	COCO+LVIS	SegF-B3-S2 <sub>384</sub>	40.14	85.45	7.03	10.74	649
SimpleClick	COCO+LVIS	ViT-B	88.5	85.11	7.47	12.39	797
SAM	SA-1B	ViT-B	<b>4.0</b>	86.16	7.46	12.42	811
FocSAM	COCO+LVIS*	ViT-H	18.6	88.6	5.74	9.44	580
InterFormer	COCO+LVIS	ViT-B	30.5	82.62	7.17	10.77	658
SegNext	COCO+LVIS	ViT-B	22.1	85.71	7.18	11.52	700
Ours	COCO+LVIS*	ViT-B	5.1	88.5	6.19	9.84	603
Ours	COCO+LVIS*	ViT-H	6.9	<b>89.6</b>	<b>5.44</b>	<b>9.16</b>	<b>566</b>
HQ-SAM	HQ-Seg*	ViT-B	4.7	89.95	6.49	10.79	671
SegNext	COCO+LVIS+HQ-Seg	ViT-B	22.1	91.75	5.32	9.42	583
Ours	COCO+LVIS+HQ-Seg*	ViT-B	5.1	92.3	4.94	8.79	538
Ours	COCO+LVIS+HQ-Seg*	ViT-H	6.9	<b>92.3</b>	<b>4.54</b>	<b>8.10</b>	<b>510</b>

### 3.4.2 Dynamic Patch Selector

Benefiting from the decoupled design and error map prediction, we are able to dynamically perform local patch updating. Unlike the FocalClick approach, which conducts a progressive merge after a fixed 10 iterations of interactions, our approach is much more efficient. We adaptively decide whether path updates are necessary by comparing the changes in error maps between each iteration of GlobalDiff Refiner. If the error map regions increase, it indicates significant influence between interactions, and we choose to use PatchDiff for local updates without altering other areas. Otherwise, we continue to use GlobalDiff.

### 3.5 Training supervision

First, We adopted Normalized Focal Loss  $L_{nfl}$  proposed in RITMSofiuk et al. [2022] to finetune the SAM decoder. Then, we used Dice Loss  $L_{dice}$  and Binary Cross Entropy Loss  $L_{bce}$  to supervise the error heads of GlobalDiff Refiner and PatchDiff Refiner. For the refined predictions, we add error region weight(1.5) on the NFL loss, denoted as  $L_{bnfl}$ .

$$\begin{aligned} \mathbf{L} = & \mathbf{L}_{nfl} + \mathbf{L}_{dice}^g + \mathbf{L}_{bce}^g + \mathbf{L}_{bnfl}^g \\ & + \mathbf{L}_{dice}^p + \mathbf{L}_{bce}^p + \mathbf{L}_{bnfl}^p \end{aligned} \quad (3)$$

where  $\mathbf{L}^g$  and  $\mathbf{L}^p$  denote the supervision for GlobalDiff Refiner and PatchDiff Refiner respectively.

## 4 Experiments

We conduct a series of experiments to test the performance of our model. We contrast our method with previous works. The experimental settings and the results of the experiments are as follows.

### 4.1 Experimental Setting

#### 4.1.1 Dataset.

We train our model on 2 different dataset configurations. For one configuration we train our model on COCO Lin et al. [2014] + LVIS Gupta et al. [2019] datasets, following previous works Huang et al. [2024a], Chen et al. [2022], Liu et al. [2023]. For this configuration, we evaluate the models’ zero-shot interactive segmentation capabilities on GrabCutRother et al. [2004], BerkeleyMcGuinness and O’connor [2010], DAVIS Perazzi et al. [2016] and SBD Hariharan et al. [2011] datasets. For another configuration, we test the performance of our method on high-precision datasets. We train our model on COCO + LVIS + HQ-Seg Ke et al. [2024] datasets. HQ-Seg dataset is a high-quality and well-annotated dataset with 44K extremely accurate image mask annotations. We test the model on the HQ-Seg dataset for this configuration.

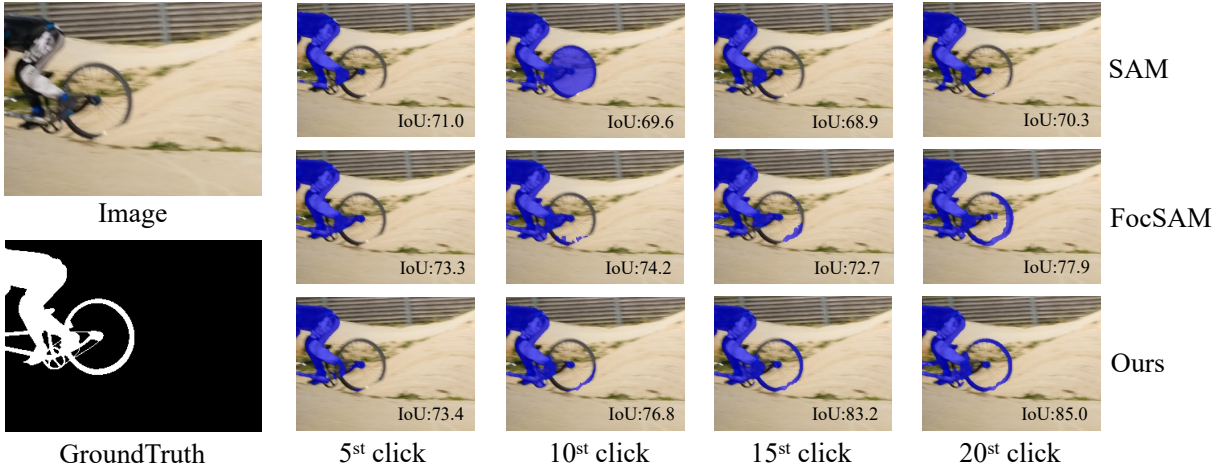


Figure 3: **Qualitative analysis on a challenge Example.** The far-left image presents a challenging example featuring the image and ground truth (GT) with blue masks. The top, middle, and bottom rows on the right respectively display the segmentation results of SAM, FocSAM and our method, at the 5th, 10th, 15th, and 20th clicks.

#### 4.1.2 Implementation details.

We utilize the pre-trained ViT-H and ViT-b from SAM Kirillov et al. [2023] as the backbone with the prompt encoder and decoder. The GlobalDiff Refiner and the PatchEdge Refiner are light-weighted convolutional neural networks, as shown in Figure 2. Training and evaluations are performed on a server with 4 NVIDIA Tesla V100-PCIE-32GB GPUs and Intel(R) Xeon(R) Gold 6278C CPU.

#### 4.1.3 Training strategy.

In the training process, we adopt the two-stage training strategy of FocSAM Huang et al. [2024a] that firstly fine-tune the SAM decoder for 320k iterations at a batch size of 4 with frozen image encoder and prompt encoder, and then train SAM-REF with the frozen decoder and frozen encoders in the same settings for 80k iterations. We adopt InterFormer’s click simulation strategy Huang et al. [2023] for interactive simulation before loss computation. Moreover, we use the image encoder to pre-extract and store the image embeddings of the datasets to reduce computational costs. This strategy greatly improves the training speed.

#### 4.1.4 Evaluation.

Following previous work, we report the results on metrics of mean Intersection over Union (mIoU), number of clicks (NoC), number of failure cases (NoF), and the Seconds Per Click (SPC) metrics on 20 clicks. And we test the latency of Segmentation Anything Task (SAT Latency) following SegNext Liu et al. [2024]. **mIoU** measures the average intersection over union (IoU) given a fixed number of consecutive interactions. We report the mIoU on 5 clicks. **NoC** measures the number of clicks required to achieve a predefined IoU. We set targets IoU of 90 and 95, and report the number of clicks to achieve the target IoUs. **NoF** measures the number of failure cases that cannot achieve the target IoU in 20 clicks. We report the failure cases on NoF95. **SPC** measures the latency of each click, which represents the speed. SPC is tested on CPU. Following SegNext Liu et al. [2024], **SAT Latency** measures the latency for the Segment Anything Task (SAT). We fix the input image size at  $1024 \times 1024$  and prompt the model with a grid of  $16 \times 16$  points. We compute the total time required to process all points by inputting one point at a time with our previous mask. SAT Latency is tested on a single GPU.

## 4.2 Main Results

In Table 1, we present the main results of SAM-REF, benchmarked against mainstream methods. Our method is based on SAM, where we freeze the SAM encoder and train only a few remaining parameters to mitigate bias inherent. We compare our model with previous early fusion and late fusion models. We are slightly weaker than SimpleClick only on the NoC95 metric of the Davis dataset. In the remaining datasets, SAM-REF achieved state-of-the-art performance in

Table 3: Ablation study for refiner. GD: GlobalDiff Refiner, PD: PatchDiff Refiner, DPS: Dynamic Patch Selector

	Method			SPC	NoC90	NoC95
	GD	PD	DPS			
1	✓			0.492	4.66	9.53
2	✓	✓		0.535	4.67	9.50
3	✓	✓	✓	0.511	<b>4.54</b>	<b>9.28</b>

Table 4: Ablation study for the number of ResBasicBlocks.

Method	SPC	NoC90	NoC95
ResBasicBlock <sub>×1</sub>	0.483	4.57	9.77
ResBasicBlock <sub>×3</sub>	0.511	<b>4.56</b>	<b>9.28</b>
ResBasicBlock <sub>×5</sub>	0.545	4.66	9.85
ResBasicBlock <sub>×8</sub>	0.710	4.61	10.21

both NOC90 and NOC95 metrics, using ViT-H as the backbone. However, as the early fusion method, SimpleClick requires a heavy image encoding at each interaction, whereas our approach is much more time-efficient. Additionally, we provide ViT-B results, showing it matches the speed and accuracy of the fastest early fusion method (FocalClick).

As a method that combines early fusion and late fusion, our approach achieves state-of-the-art accuracy compared to all late fusion methods on these datasets. Due to the additional modules, our method is slightly slower than the SAM method. However, we still maintain the low latency advantage of late fusion, as shown in Table 2. Our method effectively leverages the potential of SAM through image-prompt synergy, surpassing most specialist models while retaining SAM’s advantages.

In Table 2, we compare our method with state-of-the-art approaches on high-quality and challenging segmentation datasets. Our method outperforms others across different backbones and dataset benchmarks, while maintaining the low latency. The early fusion method cannot maintain low latency on the Segment Anything Task (SAT). InterFormer and SegNext, which rely solely dense presentation of visual prompts, are more costly than SAM’s use of the sparse representationLiu et al. [2024]. Our method combines the benefits of both prompt types. This demonstrates that our method can effectively enhance the performance of late fusion in complex scenarios, as evidenced by Qualitative Result.

## 5 Ablation Experiments

### 5.1 Component Module Analysis.

To demonstrate the effect of our model’s modules, *i.e.*, GlobalDiff Refiner, PatchDiff Refiner, and the Dynamic Patch Selector, we perform an ablation study by disabling the modules to test the efficiency and effectiveness of the model. We have set 3 experiment, one with GlobalDiff Refiner enabled, one with GlobalDiff and PatchDiff enabled, and one with the full configuration. For each experiment, we test the SPC, NoC90, and NoC95 to evaluate the speed and the accuracy.

We have shown the results in Table 3. The third experiment with full configurations achieves the best accuracy. The first experiment with only GlobalDiff Refiner enabled has the fastest calculating speed yet the minimum accuracy. By adding the PatchDiff Refiner (the second experiment), the model refines a local region of GlobalDiff’s mask, which can slightly improve the accuracy. However, the added module slows down the speed slightly. In the third experiment, the Dynamic Patch Selector enables selective use of the PatchDiff Refiner module to improve speed. It only modifies the window of the previous mask, effectively addressing interference between interactions and gradually refining the window. This ablation study has demonstrated the effectiveness and necessity of each module in our method.

### 5.2 Number of ResBasicBlocks

The table 4 shows the impact of the number of ResBasicBlocks on accuracy and speed. With three ResBasicBlocks, our method achieves the best results. Fewer blocks fail to capture details effectively, while more blocks reduce speed and harm the semantic capabilities of SAM image embeddings, thus decreasing accuracy. This experiment demonstrates the rationale for setting the number of Res-BasicBlocks to 3.

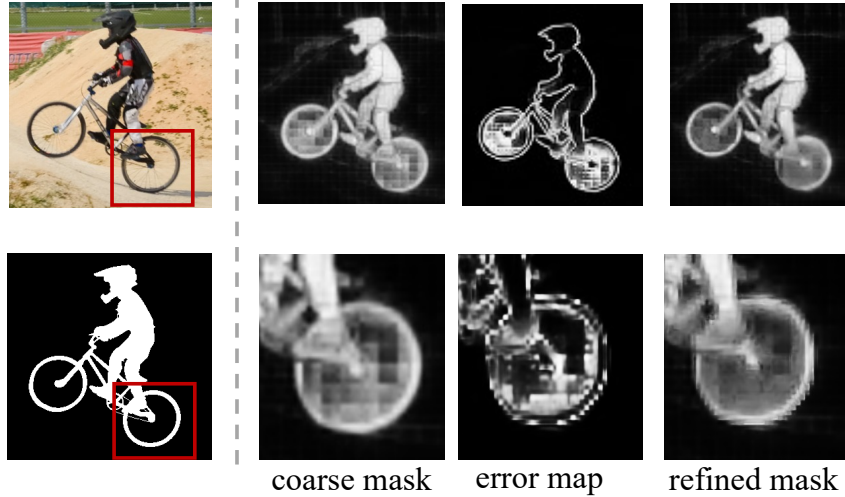


Figure 4: **Qualitative results for the effectiveness of GlobalDiff and PatchDiff Refiner.** The first row shows the global refinement results of GlobalDiff Refiner. The red box indicates the region for local refinement. The second row shows the local refinement results of PatchDiff Refiner.

## 6 Qualitative Result

In Figure 3, we show the qualitative results compared to SAM Kirillov et al. [2023] and FocSAM Huang et al. [2024a] on a challenge Example. This visualization demonstrates SAM-REF’s enhanced precision. Our method achieves the highest mIoU in all clicks. Both FocSAM and our method are trained on COCO+LVIS and freeze the SAM’s image encoder parameters. In the later clicks, our method can segment the detailed shape of the wheel, while SAM and FocSAM cannot. Based on challenging scenarios, the original SAM results are unsatisfactory. While FocSAM enhances stability and prevents progressive deterioration, it remains limited by image embeddings, potentially missing object details. Our method retrieves lost object details from the original image through image-prompt synergy.

We present the results at each stage of our method in Figure 4. The coarse mask is generated by the SAM decoder. The first row demonstrates how GlobalDiff refines the global segmentation process. The error map presents the error regions within SAM’s predicted areas. In this scenario, the error regions are concentrated around the object edges and thin structures. Then, GlobalDiff Refiner specifically refines these error regions. The second row demonstrates the refinement process of PatchDiff Refiner. It focuses on refining the areas with the largest errors between the interactions. In this image, the errors are mainly concentrated in the hollow regions.

## 7 Limitations

Late fusion methods are gradually becoming the standard pipeline for generalist models. However, in many cases, fixing the image encoder and only fine-tuning the remaining parameters has a limited effect on eliminating the inherent biases of generalist models. For interactive segmentation tasks, the mode of interaction is extremely important. Our method reintroduces image-prompt synergy, effectively enhancing the performance of generalist models on downstream data. However, there is still a slight gap compared to the best-performing early fusion models(SimpleClick), despite our approach being faster. We will leave the improvements for future work.

Our method exclusively on click-based interactive segmentation. However, we believe that reintroducing image-prompt synergy can enhance performance across various interaction forms, including boxes, scribbles, and text.

## 8 Conclusion

SAM has significantly advanced late fusion approaches in interactive segmentation. However, it lacks detailed object extraction compared to early fusion approaches. Existing late fusion methods completely overlook the importance of image and prompt synergy. Our method redesigns the SAM-based interactive segmentation pipeline, fusing images and prompts from both global and local perspectives. This adaptation fully taps into SAM’s potential for interactive

segmentation. Even in challenging scenarios, SAM-REF outperforms current state-of-the-art methods while maintaining SAM’s low latency.

## References

Qin Liu, Jaemin Cho, Mohit Bansal, and Marc Niethammer. Rethinking interactive image segmentation with low latency high quality and diverse prompts. In *Proceedings of the IEEE/CVF Conference on Computer Vision and Pattern Recognition*, pages 3773–3782, 2024.

You Huang, Zongyu Lan, Liujuan Cao, Xianming Lin, Shengchuan Zhang, Guannan Jiang, and Rongrong Ji. Focsam: Delving deeply into focused objects in segmenting anything. In *Proceedings of the IEEE/CVF Conference on Computer Vision and Pattern Recognition*, pages 3120–3130, 2024a.

Alexander Kirillov, Eric Mintun, Nikhila Ravi, Hanzi Mao, Chloe Rolland, Laura Gustafson, Tete Xiao, Spencer Whitehead, Alexander C Berg, Wan-Yen Lo, et al. Segment anything. In *Proceedings of the IEEE/CVF International Conference on Computer Vision*, pages 4015–4026, 2023.

Xi Chen, Zhiyan Zhao, Yilei Zhang, Manni Duan, Donglian Qi, and Hengshuang Zhao. Focalclick: Towards practical interactive image segmentation. In *Proceedings of the IEEE/CVF Conference on Computer Vision and Pattern Recognition*, pages 1300–1309, 2022.

You Huang, Hao Yang, Ke Sun, Shengchuan Zhang, Liujuan Cao, Guannan Jiang, and Rongrong Ji. Interformer: Real-time interactive image segmentation. In *Proceedings of the IEEE/CVF International Conference on Computer Vision*, pages 22301–22311, 2023.

Yanghao Li, Hanzi Mao, Ross Girshick, and Kaiming He. Exploring plain vision transformer backbones for object detection. In *European conference on computer vision*, pages 280–296. Springer, 2022.

Qin Liu, Zhenlin Xu, Gedas Bertasius, and Marc Niethammer. Simpleclick: Interactive image segmentation with simple vision transformers. In *Proceedings of the IEEE/CVF International Conference on Computer Vision*, pages 22290–22300, 2023.

Shoukun Sun, Min Xian, Fei Xu, Luca Capriotti, and Tiankai Yao. Cfr-ic1: Cascade-forward refinement with iterative click loss for interactive image segmentation. In *Proceedings of the AAAI Conference on Artificial Intelligence*, volume 38, pages 5017–5024, 2024.

Lei Ke, Mingqiao Ye, Martin Danelljan, Yu-Wing Tai, Chi-Keung Tang, Fisher Yu, et al. Segment anything in high quality. *Advances in Neural Information Processing Systems*, 36, 2024.

Zhaozhi Xie, Bochen Guan, Weihao Jiang, Muyang Yi, Yue Ding, Hongtao Lu, and Lei Zhang. Pa-sam: Prompt adapter sam for high-quality image segmentation. *arXiv preprint arXiv:2401.13051*, 2024.

Yann LeCun, Yoshua Bengio, and Geoffrey Hinton. Deep learning. *nature*, 521(7553):436–444, 2015.

George Barnum, Sabera Talukder, and Yisong Yue. On the benefits of early fusion in multimodal representation learning. *arXiv preprint arXiv:2011.07191*, 2020.

Alexey Dosovitskiy, Lucas Beyer, Alexander Kolesnikov, Dirk Weissenborn, Xiaohua Zhai, Thomas Unterthiner, Mostafa Dehghani, Matthias Minderer, Georg Heigold, Sylvain Gelly, et al. An image is worth 16x16 words: Transformers for image recognition at scale. *arXiv preprint arXiv:2010.11929*, 2020.

Ning Xu, Brian Price, Scott Cohen, Jimei Yang, and Thomas S Huang. Deep interactive object selection. In *Proceedings of the IEEE conference on computer vision and pattern recognition*, pages 373–381, 2016.

Konstantin Sofiuk, Ilya A Petrov, and Anton Konushin. Reviving iterative training with mask guidance for interactive segmentation. In *2022 IEEE International Conference on Image Processing (ICIP)*, pages 3141–3145. IEEE, 2022.

Zheng Lin, Zheng-Peng Duan, Zhao Zhang, Chun-Le Guo, and Ming-Ming Cheng. Focuscut: Diving into a focus view in interactive segmentation. In *Proceedings of the IEEE/CVF Conference on Computer Vision and Pattern Recognition*, pages 2637–2646, 2022.

Qin Liu, Meng Zheng, Benjamin Planche, Srikrishna Karanam, Terrence Chen, Marc Niethammer, and Ziyan Wu. Pseudoclick: Interactive image segmentation with click imitation. In *European Conference on Computer Vision*, pages 728–745. Springer, 2022.

Rodrigo Benenson, Stefan Popov, and Vittorio Ferrari. Large-scale interactive object segmentation with human annotators. In *Proceedings of the IEEE/CVF conference on computer vision and pattern recognition*, pages 11700–11709, 2019.

Xiaoke Huang, Jianfeng Wang, Yansong Tang, Zheng Zhang, Han Hu, Jiwen Lu, Lijuan Wang, and Zicheng Liu. Segment and caption anything. In *Proceedings of the IEEE/CVF Conference on Computer Vision and Pattern Recognition*, pages 13405–13417, 2024b.

Kaiming He, Xiangyu Zhang, Shaoqing Ren, and Jian Sun. Deep residual learning for image recognition. In *Proceedings of the IEEE conference on computer vision and pattern recognition*, pages 770–778, 2016.

Kaiming He, Georgia Gkioxari, Piotr Dollár, and Ross Girshick. Mask r-cnn. In *Proceedings of the IEEE international conference on computer vision*, pages 2961–2969, 2017.

Tsung-Yi Lin, Michael Maire, Serge Belongie, James Hays, Pietro Perona, Deva Ramanan, Piotr Dollár, and C Lawrence Zitnick. Microsoft coco: Common objects in context. In *Computer Vision–ECCV 2014: 13th European Conference, Zurich, Switzerland, September 6–12, 2014, Proceedings, Part V 13*, pages 740–755. Springer, 2014.

Agrim Gupta, Piotr Dollar, and Ross Girshick. Lvis: A dataset for large vocabulary instance segmentation. In *Proceedings of the IEEE/CVF conference on computer vision and pattern recognition*, pages 5356–5364, 2019.

Carsten Rother, Vladimir Kolmogorov, and Andrew Blake. " grabcut" interactive foreground extraction using iterated graph cuts. *ACM transactions on graphics (TOG)*, 23(3):309–314, 2004.

Kevin McGuinness and Noel E O’connor. A comparative evaluation of interactive segmentation algorithms. *Pattern Recognition*, 43(2):434–444, 2010.

Federico Perazzi, Jordi Pont-Tuset, Brian McWilliams, Luc Van Gool, Markus Gross, and Alexander Sorkine-Hornung. A benchmark dataset and evaluation methodology for video object segmentation. In *Proceedings of the IEEE conference on computer vision and pattern recognition*, pages 724–732, 2016.

Bharath Hariharan, Pablo Arbeláez, Lubomir Bourdev, Subhransu Maji, and Jitendra Malik. Semantic contours from inverse detectors. In *2011 international conference on computer vision*, pages 991–998. IEEE, 2011.